UV synchrotron radiation linear dichroism spectroscopy of the anti-psoriatic drug anthralin

Nguyen, Duy Duc; Jones, Nykola C.; Hoffmann, Søren V.; Spanget-Larsen, Jens

Published in:
PeerJ

DOI:
10.7717/peerj-pchem.5

Publication date:
2019

Document Version
Publisher's PDF, also known as Version of record

Citation for published version (APA):
Nguyen, D. D., Jones, N. C., Hoffmann, S. V., & Spanget-Larsen, J. (2019). UV synchrotron radiation linear dichroism spectroscopy of the anti-psoriatic drug anthralin. *PeerJ*, *2019*(1), Article 1:e5. https://doi.org/10.7717/peerj-pchem.5

PeerJ Physical Chemistry

UV synchrotron radiation linear dichroism spectroscopy of the anti-psoriatic drug anthralin

Duy Duc Nguyen[1,3], Nykola C. Jones[2], Søren Vrønning Hoffmann[2] and Jens Spanget-Larsen[1]

[1] Department of Science and Environment, Roskilde University, Roskilde, Denmark
[2] ISA, Department of Physics and Astronomy, Aarhus University, Aarhus, Denmark
[3] Current affiliation: Intertek Vietnam Limited, Ho Chi Minh City, Vietnam

ABSTRACT

Anthralin (1,8-dihydroxyanthrone, 1,8-dihydroxy-9(10*H*)-anthracenone), also known as dithranol and cignolin, is one of the most efficient drugs in the treatment of psoriasis and other skin diseases. The precise mode of biochemical action is not fully understood, but the activity of the drug is increased by the influence of UV radiation. In the present investigation, the UV absorption of anthralin is studied by synchrotron radiation linear dichroism (SRLD) spectroscopy on molecular samples partially aligned in stretched polyethylene, covering the near and vacuum UV regions with wavenumbers ranging from 23,000 to 58,000 cm^{-1} (430–170 nm). The observed polarization spectra are well predicted by quantum chemical calculations using time-dependent density functional theory (TD–DFT). About a dozen spectral features are assigned to computed electronic transitions. The calculations support interpretation of the anomalous fluorescence of anthralin as a result of barrier-less excited state intramolecular proton transfer (ESIPT) to the tautomer 8,9-dihydroxy-1(10*H*)-anthracenone.

Subjects Spectroscopy, Theoretical and Computational Chemistry, Photochemistry, Physical Chemistry
Keywords Anthralin, Electronic transitions, Polarization spectroscopy, Linear dichroism (LD), Excited state intramolecular proton transfer (ESIPT), Synchrotron radiation, Time-dependent density functional theory (TD-DFT)

Submitted 25 September 2019
Accepted 18 October 2019
Published 15 November 2019

Corresponding author
Jens Spanget-Larsen, spanget@ruc.dk

Academic editor
Walter de Azevedo Jr.

Additional Information and Declarations can be found on page 11

DOI **10.7717/peerj-pchem.5**

INTRODUCTION

For more than 100 years anthralin (**A**), also known as dithranol and cignolin, has been applied as an effective topical agent for the treatment of the skin disease psoriasis (*Ashton et al., 1983*; *Van de Kerkhof, 1991*; *Sehgal, Verma & Khurana, 2014*; *Körber et al., 2019*). The compound was for many years believed to be anthracene-1,8,9-triol, but spectroscopic and crystallographic analyses indicated that the prevailing constitution is that of the tautomer 1,8-dihydroxy-9(10*H*)-anthracenone (*Hellier & Whitefield, 1967*; *Avdovich & Neville, 1980*; *Ahmed, 1980*), see Fig. 1. **A** is a reactive compound characterized by complicated red-ox properties (*Czerwinska et al., 2006*; *Pshenichnyuk & Komolov, 2014*) and it exhibits anomalous fluorescence with a Stokes shift of 10,500 cm^{-1}, indicating large rearrangement in the excited state (*Møller et al., 1998*). The precise mode of biochemical action is not fully understood, but the application of UV radiation is known to increase

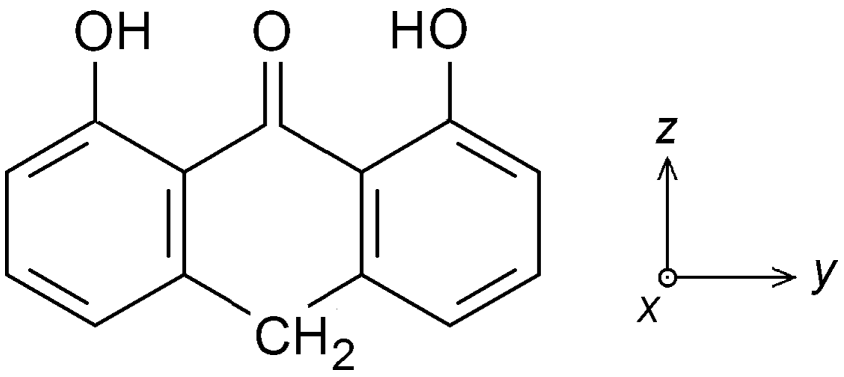

Figure 1 **Anthralin (A) with definition of the molecular coordinate system.**
Full-size DOI: 10.7717/peerjpchem.5/fig-1

the activity of the drug (*Lapolla et al., 2011*). Bally and coworkers (*Czerwinska et al., 2006*) and *Pshenichnyuk & Komolov (2014)* thus considered the involvement of excited electronic states generated by UV irradiation.

In the present work, we investigate the excited states of **A** by synchrotron radiation linear dichroism (SRLD) UV spectroscopy on molecular samples partially aligned in stretched low-density polyethylene (PE). The use of synchrotron radiation (*Miles et al., 2007*; *Miles et al., 2008*) provides increased signal-to-noise ratio in the UV region and enables a significant expansion of the accessible spectral range, compared with the use of a traditional light source (*Nguyen et al., 2018*; *Nguyen et al., 2019*). In the present study, the measurement is extended into the vacuum UV, covering the region up to 58,000 cm^{-1} (170 nm); this is an extension of the previously investigated range by about 11,000 cm^{-1} (1.4 eV) (*Andersen & Spanget-Larsen, 1997*). Linear dichroism (LD) spectroscopy yields experimental information on the molecular transition moment directions of the observed absorption bands (*Michl & Thulstrup, 1986*; *Thulstrup & Michl, 1989*; *Rodger & Nordén, 1997*; *Nordén, Rodger & Dafforn, 2010*). The observed spectra are discussed with reference to the results of time-dependent density functional theory (TD-DFT) calculations (*Marques et al., 2012*; *Foresman & Frisch, 2015*). Additional information is provided as Supplemental Files.

MATERIALS & METHODS

Sample preparation

A sample of **A** (CAS No. 1143-38-0) was purchased from Sigma-Aldrich and purified by column chromatography as previously described (*Andersen & Spanget-Larsen, 1997*). The near-UV absorbance spectrum of the purified substance in *n*-heptane solution (Merck Uvasol) is shown in Fig. S1. Low-density polyethylene (PE) 100 μm sheet material was obtained from Hinnum Plast A/S. A 2.5×6 cm PE piece cut from the sheet was purified by extraction with chloroform (Merck Uvasol) at 50 °C for one day. **A** was introduced by submersion of the dried PE sample into a saturated chloroform solution of the substance in a sealed container at room temperature for three days. After evaporation of the chloroform

from the doped sample, the surface was cleaned with ethanol (Merck Uvasol) to remove crystalline deposits. The PE sample was finally uniaxially stretched by 500%. A sample without solute was produced in the same manner for use as a reference. Further details on stretched polyethylene samples can be found in the literature (*Michl & Thulstrup, 1986*; *Thulstrup & Michl, 1989*).

Linear dichroism (LD) spectroscopy

LD spectra in the range 31,300–20,000 cm^{-1} (320–500 nm) were recorded on a UV-2101PC Shimadzu spectrophotometer at Roskilde University. SRLD spectra were measured in the range 58,000–31,300 cm^{-1} (170–320 nm) on the CD1 beamline (*Miles et al., 2007*; *Miles et al., 2008*) at the storage ring ASTRID at the Centre for Storage Ring Facilities (ISA). As previously described (*Andersen & Spanget-Larsen, 1997*; *Nguyen et al., 2018*; *Nguyen et al., 2019*), two absorbance curves were recorded at room temperature with the electric vector of the sample beam parallel (U) and perpendicular (V) to the stretching direction of the PE sample. The observed baseline-corrected LD absorbance curves $E_U(\tilde{\nu})$ and $E_V(\tilde{\nu})$ are shown in Fig. 2A. The isotropic absorbance curve $A_{ISO}(\tilde{\nu}) = E_U(\tilde{\nu}) + 2E_V(\tilde{\nu})$ is shown in Fig. S2.

Calculations

Quantum chemical calculations considering isolated molecules in the gas phase were performed by using the Gaussian16 software package (*Frisch et al., 2016*). Optimizations of molecular geometry were performed with B3LYP (*Becke, 1993*; *Lee, Yang & Parr, 1988*). This DFT was found to be very successful in the prediction of molecular and vibrational structures of compounds like **A** with intramolecular C=O···HO hydrogen bonding (*Spanget-Larsen, Hansen & Hansen, 2011*; *Hansen & Spanget-Larsen, 2012*). Geometry optimizations for the ground state (S_0) and the lowest excited singlet state (S_1) of **A** were carried out with B3LYP and TD-B3LYP, respectively, using the 6-31+G(d,p) basis set (*Foresman & Frisch, 2015*; *Frisch et al., 2016*). Vertical electronic transitions from the ground state to the 60 lowest excited singlet states were computed with TD–CAM-B3LYP (*Yanai, Tew & Handy, 2004*) and the basis set aug-cc-pVTZ (*Dunning Jr, 1989*; *Kendall, Dunning Jr & Harrison, 1992*). We recently found that this long-range corrected procedure is adequate in the prediction of electronic transitions of aromatic chromophores in the near and vacuum UV regions (*Nguyen et al., 2018*; *Nguyen et al., 2019*). A constant term was subtracted from the excitation wavenumbers calculated with TD–CAM-B3LYP in order to facilitate comparison with the observed spectra (*Grimme, 2004*; *Nguyen et al., 2018*; *Nguyen et al., 2019*); an empirical correction of 3,500 cm^{-1} was found to be adequate in the present case. The main predicted transitions are listed in Table 1 together with the observed ones. A complete listing of the calculated transitions is provided as Data S1. Graphical representations of transitions to $^1A_1$ and $^1B_2$ states are shown in Fig. 3. Gaussian convolutions considering all allowed transitions are provided as Fig. S3, using previously described procedures (*Serr & O'Boyle, 2009*; *Nguyen et al., 2019*). Detailed results for the ESIPT photoproduct 8,9-dihydroxy-1(10*H*)-anthracenone are given in Data S2, results for additional excited state configurations are outlined in Fig. S4.

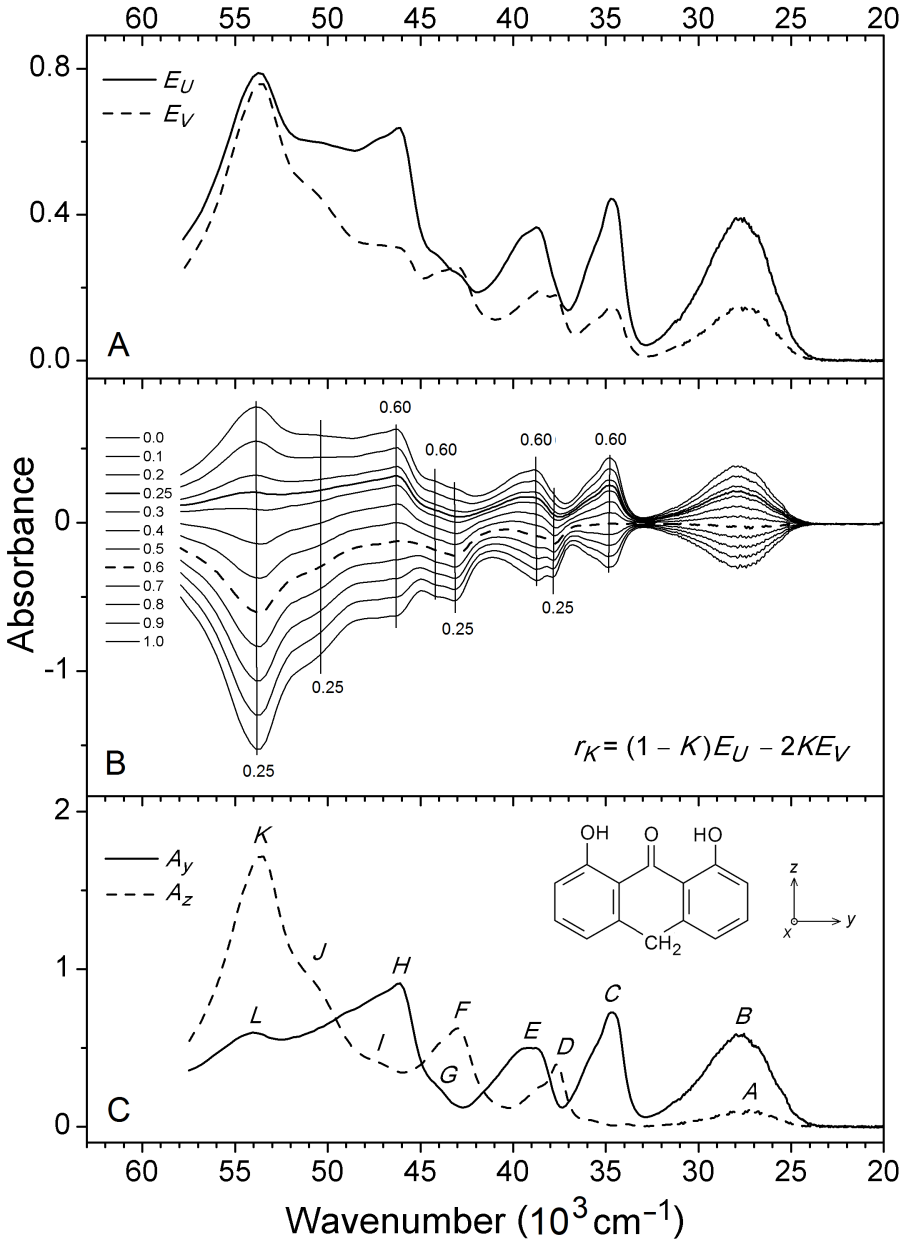

Figure 2 **Observed SRLD absorbance curves.** (A) Absorbance curves E_U and E_V for anthralin (**A**) partially aligned in uniaxially stretched polyethylene, indicating absorbance measured with linearly polarized radiation with electric vector parallel and perpendicular, respectively, to the stretching direction U of the polymer. (B) Family of reduced absorbance curves r_K according to Eq. (2) with K varying from 0.0 to 1.0 in steps of 0.1. Orientation factors K determined for prominent features are indicated. (C) Partial absorbance curves A_y and A_z according to Eq. (3) corresponding to absorbance polarized along the molecular axes y and z, see text.

Full-size DOI: 10.7717/peerjpchem.5/fig-2

Table 1 Observed features of the SRLD spectrum of anthralin (A) and theoretical electronic transitions predicted with TD–CAM-B3LYP/aug-cc-pVTZ.

	Observed			TD–CAM-B3LYP[a]			
	$\tilde{\nu}$[b]	Abs[c]	Pol[d]	Term	$\tilde{\nu}$[b,e]	f[f]	Leading configurations[g]
A	27.3	0.11	*z*	$2\,^1A_1$	27.9	0.03	93% $[6b_1(\pi)\rightarrow 7b_1(\pi^*)]$
B	27.7	0.58	*y*	$1\,^1B_2$	27.7	0.29	94% $[4a_2(\pi)\rightarrow 7b_1(\pi^*)]$
C	34.6	0.73	*y*	$2\,^1B_2$	34.6	0.08	79% $[3a_2(\pi)\rightarrow 7b_1(\pi^*)]$, 13% $[6b_1(\pi)\rightarrow 5a_2(\pi^*)]$
D	37.6	0.39	*z*	$3\,^1A_1$	38.6	0.03	73% $[5b_1(\pi)\rightarrow 7b_1(\pi^*)]$, 13% $[6b_1(\pi)\rightarrow 8b_1(\pi^*)]$
E	39.2	0.50	*y*	$3\,^1B_2$	40.9	0.18	54% $[6b_1(\pi)\rightarrow 5a_2(\pi^*)]$, 17% $[3a_2(\pi)\rightarrow 7b_1(\pi^*)]$
F	42.9	0.62	*z*	$5\,^1A_1$	43.2	0.23	56% $[6b_1(\pi)\rightarrow 8b_1(\pi^*)]$, 21% $[5b_1(\pi)\rightarrow 7b_1(\pi^*)]$
G	44	(0.2)	*y*	$4\,^1B_2$	43.5	0.03	55% $[4a_2(\pi)\rightarrow 8b_1(\pi^*)]$, 23% $[6b_1(\pi)\rightarrow 6a_2(\pi^*)]$
H	46.1	0.91	*y*	$5\,^1B_2$	47.4	0.52	29% $[3a_2(\pi)\rightarrow 8b_1(\pi^*)]$, 19% $[6b_1(\pi)\rightarrow 6a_2(\pi^*)]$
I	47	(0.4)	*z*	$7\,^1A_1$	50.9	0.06	43% $[6b_1(\pi)\rightarrow 9b_1(\pi^*)]$, 16% $[5b_1(\pi)\rightarrow 8b_1(\pi^*)]$
J	51	(1.0)	*z*	$8\,^1A_1$	52.1	0.17	21% $[5b_1(\pi)\rightarrow 8b_1(\pi^*)]$, 19% $[4b_1(\pi)\rightarrow 7b_1(\pi^*)]$
K	53.4	1.72	*z*	$9\,^1A_1$	52.8	0.41	53% $[4a_2(\pi)\rightarrow 6a_2(\pi^*)]$, 30% $[3a_2(\pi)\rightarrow 5a_2(\pi^*)]$
				$10\,^1A_1$	55.3	0.09	66% $[4b_1(\pi)\rightarrow 7b_1(\pi^*)]$, 12% $[5b_1(\pi)\rightarrow 8b_1(\pi^*)]$
				$12\,^1A_1$	57.9	0.08	54% $[3a_2(\pi)\rightarrow 6a_2(\pi^*)]$, 29% $[5b_1(\pi)\rightarrow 8b_1(\pi^*)]$
L	54.1	0.60	*y*	$8\,^1B_2$	52.5	0.16	34% $[3a_2(\pi)\rightarrow 8b_1(\pi^*)]$, 29% $[5b_1(\pi)\rightarrow 5a_2(\pi^*)]$
				$9\,^1B_2$	56.3	0.14	50% $[2a_2(\pi)\rightarrow 7b_1(\pi^*)]$, 12% $[22b_2(\sigma)\rightarrow 30a_1(\sigma^*)]$

Notes.

[a]Main transitions only. Complete list of calculated transitions provided as Data S1.
[b]Peak wavenumber in 1,000 cm^{-1}.
[c]Peak absorbance estimated from the partial absorbance curves in Fig. 2C. Entries in parentheses indicate diffuse shoulders.
[d]Polarization direction.
[e]An empirical correction of 3,500 cm^{-1} has been subtracted from the calculated wavenumber.
[f]Oscillator strength.
[g]MO energies and diagrams in Fig. 4.

RESULTS AND DISCUSSION

Linear dichroism: orientation factors and partial absorbance curves

The observed SRLD absorption curves $E_U(\tilde{\nu})$ and $E_V(\tilde{\nu})$ for **A** partially aligned in stretched PE are shown in Fig. 2A. The directional information that can be extracted from these curves is represented by the orientation factors K_i for the molecular transition moment vectors $\vec{M}_i$ of the observed spectroscopic features i (*Michl & Thulstrup, 1986*; *Thulstrup & Michl, 1989*):

$$K_i = \left\langle \cos^2\left(\vec{M}_i, U\right)\right\rangle. \tag{1}$$

The orientation factor is defined as an average over all solute molecules in the light path, indicated by the pointed brackets in Eq. (1), where $\left(\vec{M}_i, U\right)$ is the angle of the moment vector of transition i with the polymer stretching direction, U. The K_i values may be determined by the graphical TEM procedure (*Michl & Thulstrup, 1986*; *Thulstrup & Michl, 1989*) which involves construction of linear combinations of $E_U(\tilde{\nu})$ and $E_V(\tilde{\nu})$. In the present application we consider the reduced absorbance curves $r_K(\tilde{\nu})$ (*Madsen et al., 1992*):

$$r_K(\tilde{\nu}) = (1-K)E_U(\tilde{\nu}) - 2KE_V(\tilde{\nu}). \tag{2}$$

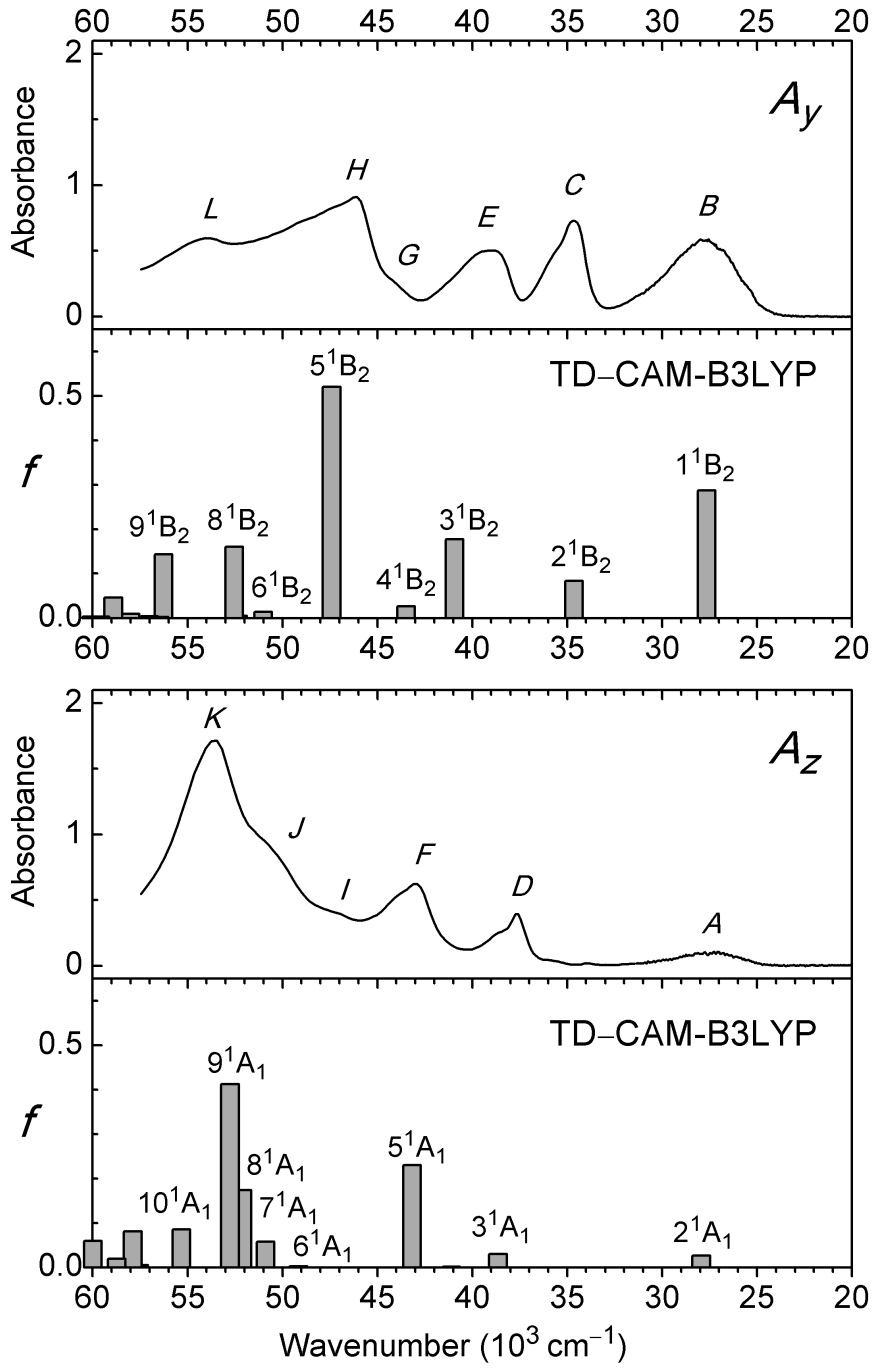

Figure 3 Partial absorbance curves A_y and A_z for anthralin (A) and electronic transitions to excited $^1B_2$ and $^1A_1$ states predicted with TD–CAM-B3LYP/aug-cc-pVTZ.

Full-size DOI: 10.7717/peerjpchem.5/fig-3

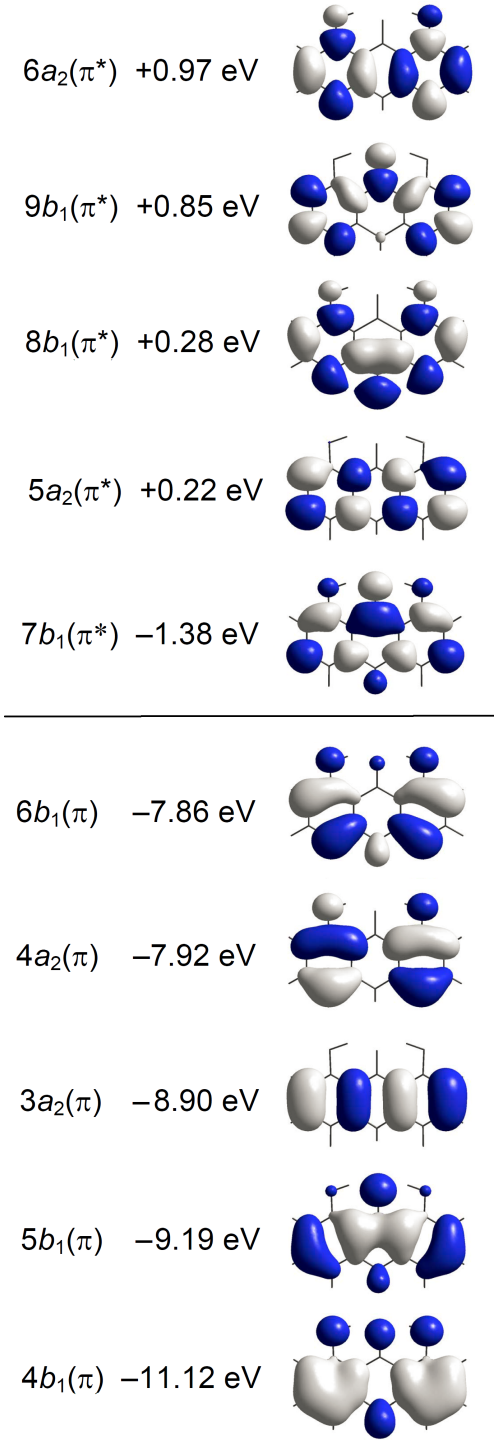

Figure 4 Energies and amplitude diagrams for the five highest occupied and five lowest unoccupied π type MOs of anthralin (A) computed with CAM-B3LYP/aug-cc-pVTZ. Different colors indicate amplitudes of different sign.

Full-size DOI: 10.7717/peerjpchem.5/fig-4

A family of curves $r_K(\tilde{\nu})$ for **A** is shown in Fig. 2B. A spectral peak or shoulder due to transition i disappears from the linear combination $r_K(\tilde{\nu})$ for $K = K_i$ and the K_i value can thus be determined by visual inspection. The molecular point group of **A** is C_{2v} (*Ahmed, 1980*) and allowed vertical transitions must be polarized along the three symmetry axes x, y, and z, corresponding to excited states of B_1, B_2, and A_1 symmetry, respectively. Hence, only three different K_i values corresponding to K_x, K_y, and K_z are expected. From the $r_K(\tilde{\nu})$ curves in Fig. 2B K values close to 0.60 can be estimated for the features at 34,600, 39,200, 44,000 and 46,100 cm^{-1}, and values close to 0.25 for those at 37,600, 42,900, 51,000 and 53,400 cm^{-1}. As previously discussed (*Andersen & Spanget-Larsen, 1997*), the relatively broad band with maximum close to 27,500 cm^{-1} (~365 nm) is due to two near-degenerate, differently polarized transitions; their K values cannot be determined directly.

The K values 0.60 and 0.25 must be assigned to K_y and K_z, corresponding to transitions polarized along the in-plane long and short molecular axes y and z. Under the assumption that absorbance polarized along the out-of-plane x axis is negligible in the present spectra, it is possible to construct the partial absorbance curves $A_y(\tilde{\nu})$ and $A_z(\tilde{\nu})$ indicating y- and z- polarized intensity (*Madsen et al., 1992*):

$$\begin{aligned} A_y(\tilde{\nu}) &= \left(K_y - K_z\right)^{-1} \cdot r_{K_z}(\tilde{\nu}) \\ A_z(\tilde{\nu}) &= \left(K_z - K_y\right)^{-1} \cdot r_{K_y}(\tilde{\nu}). \end{aligned} \tag{3}$$

The curves $A_y(\tilde{\nu})$ and $A_z(\tilde{\nu})$ produced with $(K_y, K_z) = (0.60, 0.25)$ are shown in Fig. 2C and in Fig. 3. They are shown on an expanded absorbance scale in Fig. S2, together with the isotropic absorbance curve $A_{ISO}(\tilde{\nu}) = A_y(\tilde{\nu}) + A_z(\tilde{\nu}) = E_U(\tilde{\nu}) + 2E_V(\tilde{\nu})$. The latter is equal to three times the absorbance that would have been measured in an isotropic experiment on the same sample. Six long-axis (y) polarized features *B*, *C*, *E*, *G*, *H*, and *L* and six short-axis (z) polarized features *A*, *D*, *F*, *I*, *J*, and *K* are indicated. Observed peak wavenumbers, absorbances, and polarization directions are listed in Table 1.

Electronic transitions

The spectrum starts with a relatively broad band system with maximum close to 27,500 cm^{-1} (364 nm). The absorbance is predominantly long-axis (y) polarized, overlapping weaker short-axis (z) polarized intensity. The short-axis polarized absorbance *A* with maximum at 27,300 cm^{-1} (366 nm) can be assigned to the 2^1A_1 state computed at 27,900 cm^{-1} (Table 1, Fig. 3). The computed transition is well described by promotion of an electron from the $6b_1(\pi)$ HOMO to the $7b_1(\pi^*)$ LUMO. The intense long-axis polarized band *B* peaking at 27,700 cm^{-1} (361 nm) is assigned to the 1^1B_2 state predicted at 27,700 cm^{-1} (Table 1, Fig. 3). This transition is primarily due to the promotion from the $4a_2(\pi)$ SHOMO to the $7b_1(\pi^*)$ LUMO.

Band *C* with maximum at 34,600 cm^{-1} (289 nm) is purely long-axis (y) polarized and is easily assigned to the 2^1B_2 state computed at 34,600 cm^{-1} (Table 1, Fig. 3). The following absorbance band is resolved into two differently polarized components, *D* and *E* at 37,600 and 39,200 cm^{-1} (266 and 255 nm). They can be assigned to the 3^1A_1 and 3^1B_2 states computed at 38,600 and 40,900 cm^{-1} (Table 1, Fig. 3). Band *F* at 42,900 cm^{-1} (233

nm) is predominantly short-axis (z) polarized and is assigned to the 5^1A_1 state predicted at 43,200 cm^{-1} (Table 1, Fig. 3). The band overlaps the onset of long-axis polarized (y) intensity G around 44,000 cm^{-1} (~227 nm). This feature is possibly due to the 4^1B_2 state computed at 43,500 cm^{-1} (Table 1, Fig. 3), but it may also involve b_2 symmetric vibrational components of band F, gaining long-axis polarized intensity by vibronic coupling with the strong band H. In the isotropic spectrum recorded in n-heptane solution, transition F apparently corresponds to the shoulder close to 43,500 cm^{-1} and transition G to the peak at 44,300 cm^{-1} (Fig. S1).

Assignment of individual transitions in the high-wavenumber region is complicated by the presence of broad, overlapping bands and by a high density of electronic states. Our TD–CAM-B3LYP calculation predicts about 50 electronic transitions between 60,000 and 45,000 cm^{-1} (Data S1). In addition, the applied theoretical model may be less accurate in this region and the suggested assignments of observed features to computed transitions are necessarily tentative.

The observed long-axis (y) polarized absorbance in this region displays a strong band H with maximum at 46,100 cm^{-1} (217 nm). According to the calculated transitions, this band can be assigned to the 5^1B_2 state predicted at 47,400 cm^{-1} (Table 1, Fig. 3). Band H has a long tail into the vacuum UV with an additional peak L at 54,100 cm^{-1} (185 nm). Several states are predicted to contribute to this absorption, primarily 8^1B_2 and 9^1B_2 computed at 52,500 and 56,300 cm^{-1} (Table 1, Fig. 3).

The short-axis (z) polarized intensity in this region is dominated by a very strong band K with maximum at 53,400 cm^{-1} (187 nm) in the vacuum UV. This is the strongest absorbance observed in the investigated spectral range. The peak K at 53,400 cm^{-1} is preceded by two diffuse shoulders I and J at 47,000 and 51,000 cm^{-1} (213 and 196 nm). Several states are predicted to contribute to this band system, such as 7^1A_1, 8^1A_1, 9^1A_1, and 10^1A_1, with transition to the 9^1A_1 state computed at 52,800 cm^{-1} as the most intense (Table 1, Fig. 3).

Excited state intramolecular proton transfer (ESIPT)

The observed fluorescence emission of **A** in n-hexane solution has a maximum at 17,500 cm^{-1} (570 nm) with an unusually large Stokes shift of 10,500 cm^{-1} relative to the excitation observed at 28,000 cm^{-1} (360 nm) (*Møller et al., 1998*). The fluorescence quantum yield is nearly independent of temperature which suggests that the decay from the initially formed excited state to the ground state does not involve barrier crossing (*Møller et al., 1998*).

According to the orbital amplitudes in Fig. 4, the promotions $6b_1(\pi) \rightarrow 7b_1(\pi^*)$ and $4a_2(\pi) \rightarrow 7b_1(\pi^*)$ involved in the transitions to the two lowest, near-degenerate singlet states 2^1A_1 and 1^1B_2 are associated with substantial transfer of electron density from the phenolic moieties to the carbonyl group. This is expected to affect the balance of forces involved in the intramolecular hydrogen bonding, facilitating excited state intramolecular proton transfer (ESIPT) (*Andersen & Spanget-Larsen, 1997*). Geometry optimization of the excited S_1 state with TD-B3LYP predicts barrier-less transition to the ESIPT product 8,9-dihydroxy-1(10H)-anthracenone, see Fig. 5, leading to good agreement with the observed fluorescence and excitation wavenumbers (the predicted excitation wavenumber indicated

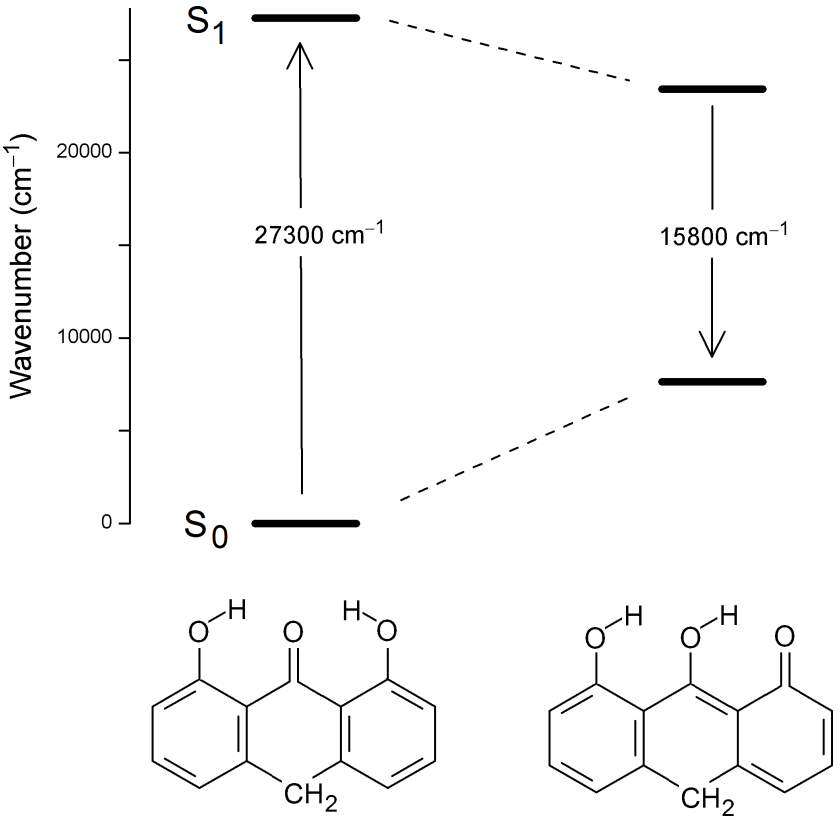

Figure 5 Predicted vertical excitation and emission wavenumbers for anthralin (A). On the left the predicted vertical transition from the ground state to the lowest excited singlet state is indicated, to the right the vertical emission from the photoproduct 8,9-dihydroxy-1(10*H*)-anthracenone (TD-B3LYP/6-31+G(d,p)). The predicted photoproduct is a result of barrier-less excited state intramolecular proton transfer (ESIPT). Further details are provided in Data S2 and Fig. S4.

Full-size DOI: 10.7717/peerjpchem.5/fig-5

in Fig. 5 is slightly different from the one listed in Table 1 because of different TD-DFT procedures). The present TD-DFT results thus support the assignment previously suggested on the basis of semi-empirical model calculations (*Andersen & Spanget-Larsen, 1997*; *Møller et al., 1998*). Excited state equilibrium nuclear coordinates and other computational data for the ESIPT product are provided as Data S2; relative energies of this and additional excited state configurations are outlined in Fig. S4.

A similar excited state rearrangement is observed for the closely related compound 1,8-dihydroxy-9,10-anthraquinone (chrysazin, an oxidation product of **A**) as reported by Smulevich and coworkers (*Smulevich et al., 1987*; *Marzocchi et al., 1998*) and recently studied theoretically by *Mohammed et al. (2014)* and by *Zheng, Zhang & Zhao (2017)*.

CONCLUSIONS

In this study, polarization data for the anti-psoriatic drug anthralin (**A**) is provided by SRLD spectroscopy in the region 58,000–23,000 cm^{-1} (170–430 nm), leading to the resolution of otherwise overlapping absorption bands and to experimental symmetry assignments of the

observed transitions. The results of the present TD–DFT calculations account admiringly well for the observed polarization spectra throughout the investigated spectral range, allowing detailed assignments of about a dozen observed spectral features to computed electronic states. Assignment of the anomalous fluorescence of **A** to the ESIPT product 8,9-dihydroxy-1(10*H*)-anthracenone is supported by the present theoretical results.

ACKNOWLEDGEMENTS

This paper honours the memory of Professor Erik Waaben Thulstrup and his fundamental contributions to the development of linear dichroism spectroscopy. The authors are grateful to Eva M. Karlsen for technical assistance.

ADDITIONAL INFORMATION AND DECLARATIONS

Funding

This work was supported by grants of beam time on the CD1 beamline at ISA. The stay of Duy Duc Nguyen at Roskilde University was enabled by a Ph.D. scholarship awarded by the Vietnamese Ministry of Education and Training. Additional support was provided by the Danish International Development Agency (DANIDA) via the Enhancement of Research Capacity (ENRECA) program. The funders had no role in study design, data collection and analysis, decision to publish, or preparation of the manuscript.

Grant Disclosures

The following grant information was disclosed by the authors:
CD1 beamline at ISA.
Duy Duc Nguyen at Roskilde University.
Danish International Development Agency (DANIDA).

Competing Interests

The authors declare there are no competing interests.

Author Contributions

- Duy Duc Nguyen conceived and designed the experiments, performed the experiments, analyzed the data, authored or reviewed drafts of the paper, approved the final draft.
- Nykola C. Jones and Søren Vrønning Hoffmann conceived and designed the experiments, performed the experiments, contributed reagents/materials/analysis tools, authored or reviewed drafts of the paper, approved the final draft.
- Jens Spanget-Larsen conceived and designed the experiments, analyzed the data, contributed reagents/materials/analysis tools, prepared figures and/or tables, performed the computation work, authored or reviewed drafts of the paper, approved the final draft.

Data Availability

The following information was supplied regarding data availability:

The raw data are available in the Supplemental Files.

Supplemental Information

Supplemental information for this article can be found online at http://dx.doi.org/10.7717/peerj-pchem.5#supplemental-information.

REFERENCES

Ahmed FR. 1980. The correct structural formula for anthralin. *Acta Crystallographica B* **36**:3184–3186 DOI 10.1107/S0567740880011247.

Andersen KB, Spanget-Larsen J. 1997. Electronic transitions and intramolecular hydrogen bonding in anthralin. UV–VIS linear dichroism spectroscopy and quantum chemical calculations. *Spectrochimica Acta* **53**:2615–2625 DOI 10.1016/S1386-1425(97)00198-4.

Ashton RE, Andre P, Lowe NJ, Whitefield M. 1983. Anthralin: historical and current perspectives. *Jornal of American Academy of Dermatology* **4**:173–192.

Avdovich HW, Neville GA. 1980. 1, 8-Dihydroxy-9-anthrone, the revised structure for anthralin, a USP reference-standard. *Canadian Journal of Spectroscopy* **25**:110–113.

Becke AD. 1993. Density-functional thermochemistry. III. The role of exact exchange. *Journal of Chemical Physics* **98**:5648–5652 DOI 10.1063/1.464913.

Czerwinska A, Sikora A, Szajerski P, Zielonka J, Adamus J, Marcinek A, Piech K, Bednarek P, Bally T. 2006. Anthralin: primary products of its redox reactions. *Journal of Organic Chemistry* **71**:5312–5319 DOI 10.1021/jo060622o.

Dunning Jr TH. 1989. Gaussian basis sets for use in correlated molecular calculations. I. The atoms boron through neon and hydrogen. *Journal of Chemical Physics* **90**:1007–1023 DOI 10.1063/1.456153.

Foresman JB, Frisch Æ. 2015. *Exploring chemistry with electronic structure methods*. 3rd Edition. Wallingford CT: Gaussian, Inc.

Frisch MJ, Trucks GW, Schlegel HB, Scuseria GE, Robb MA, Cheeseman JR, Scalmani G, Barone V, Petersson GA, Nakatsuji H, Li X, Caricato M, Marenich AV, Bloino J, Janesko BG, Gomperts R, Mennucci B, Hratchian HP, Ortiz JV, Izmaylov AF, Sonnenberg JL, Williams-Young D, Ding F, Lipparini F, Egidi F, Goings J, Peng B, Petrone A, Henderson T, Ranasinghe D, Zakrzewski VG, Gao J, Rega N, Zheng G, Liang W, Hada M, Ehara M, Toyota K, Fukuda R, Hasegawa J, Ishida M, Nakajima T, Honda Y, Kitao O, Nakai H, Vreven T, Throssell K, Montgomery Jr JA, Peralta JE, Ogliaro F, Bearpark MJ, J Heyd JJ, Brothers EN, Kudin KN, Staroverov VN, Keith TA, Kobayashi R, Normand J, Raghavachari K, Rendell AP, Burant JC, Iyengar SS, Tomasi J, Cossi M, Millam JM, Klene M, Adamo C, Cammi R, Ochterski JW, Martin RL, Morokuma K, Farkas O, Foresman JB, Fox DJ. 2016. *Gaussian*16 , *Revision A.03*. Wallingford CT: Gaussian, Inc.

Grimme S. 2004. Calculation of the electronic spectra of large molecules. *Reviews in Computational Chemistry* **20**:153–218.

Hansen PE, Spanget-Larsen J. 2012. On prediction of OH stretching frequencies in intramolecularly hydrogen bonded systems. *Journal of Molecular Structure* **1018**:8–13 DOI 10.1016/j.molstruc.2012.01.011.

Hellier FF, Whitefield M. 1967. The treatment of psoriasis with triacetoxyanthracene. *British Journal of Dermatology* **79**:491–496 DOI 10.1111/j.1365-2133.1967.tb11537.x.

Kendall RA, Dunning Jr TH, Harrison RJ. 1992. Electron affinities of the first-row atoms revisited. Systematic basis sets and wave functions. *Journal of Chemical Physics* **96**:6796–6806 DOI 10.1063/1.462569.

Körber A, Wilsmann-Theis D, Augustin M, Von Kiedrowski R, Mrowietz U, Rosenbach T, Meller S, Pinter A, Sticherling M, Gerdes S. 2019. Topische Therapie bei Psoriasis vulgaris—ein Behandlungspfad. *Journal der Deutschen Dermatologischen Gesellschaft* **17**:3–14.

Lapolla W, Yentzer BA, Bagel J, Halvorson CR, Feldman SR. 2011. A review of phototherapy protocols for psoriasis treatment. *Journal of the American Academy of Dermatology* **64**:936–949 DOI 10.1016/j.jaad.2009.12.054.

Lee C, Yang W, Parr RG. 1988. Development of the Colle-Salvetti correlation-energy formula into a functional of the electron density. *Physical Review B* **37**:785–789 DOI 10.1103/PhysRevB.37.785.

Madsen F, Terpager I, Olskær K, Spanget-Larsen J. 1992. Ultraviolet–visible and infrared linear dichroism spectroscopy of 1, 8-dihydroxy-9, 10-anthraquinone aligned in stretched polyethylene. *Chemical Physics* **165**:351–360 DOI 10.1016/0301-0104(92)87050-J.

Marques MAL, Maitra NT, Nogueira FMS, Gross EKU, Rubio A (eds.) 2012. *Fundamentals of time-dependent density functional theory*. *Lecture Notes in Physics 837*, Berlin: Springer.

Marzocchi MP, Mantini AR, Casu M, Smulevich G. 1998. Intramolecular hydrogen bonding and excited state proton transfer in hydroxyanthraquinones as studied by electronic spectra, resonance Raman scattering, and transform analysis. *Journal of Chemical Physics* **108**:534–549 DOI 10.1063/1.475417.

Michl J, Thulstrup EW. 1986. *Spectroscopy with polarized light. Solute alignment by photoselection, in liquid crystals, polymers and membranes.* Dearfield Beach: VCH-Wiley.

Miles AJ, Hoffmann SV, Tao Y, Janes RW, Wallace BA. 2007. Synchrotron radiation circular dichroism (SRCD) spectroscopy: new beamlines and new applications in biology. *Spectroscopy* **21**:245–255 DOI 10.1155/2007/282713.

Miles AJ, Janes RW, Brown A, Clarke DT, Sutherland JC, Tao Y, Wallace BA, Hoffmann SV. 2008. Light flux density threshold at which protein denaturation is induced by synchrotron radiation circular dichroism beamlines. *Journal of Synchrotron Radiation* **15**:420–422 DOI 10.1107/S0909049508009606.

Mohammed OF, Xiao D, Batista VS, Nibbering ETJ. 2014. Excited-state intramolecular hydrogen transfer (ESIHT) of 1, 8-dihydroxy-9, 10-anthraquinone (DHAQ) characterized by ultrafast electronic and vibrational spectroscopy and computational modeling. *The Journal of Physical Chemistry A* **118**:3090–3099 DOI 10.1021/jp501612f.

Møller S, Andersen KB, Spanget-Larsen J, Waluk J. 1998. Excited-state intramolecular proton transfer in anthralin. Quantum chemical calculations and fluorescence spectra. *Chemical Physics Letters* **291**:51–56 DOI 10.1016/S0009-2614(98)00546-6.

Nguyen DD, Jones NC, Hoffmann SV, Spanget-Larsen J. 2018. Vacuum UV polarization spectroscopy of *p*-Terphenyl. *The Journal of Physical Chemistry A* **122**:184–191 DOI 10.1021/acs.jpca.7b10442.

Nguyen DD, Jones NC, Hoffmann SV, Spanget-Larsen J. 2019. Electronic states of dibenzo-*p*-dioxin. A synchrotron radiation linear dichroism investigation. *Chemical Physics* **519**:64–68 DOI 10.1016/j.chemphys.2018.12.003.

Nordén B, Rodger A, Dafforn T. 2010. *Linear dichroism and circular dichroism: a textbook on polarized-light spectroscopy*. Cambridge: RCS Publishing.

Pshenichnyuk SA, Komolov AS. 2014. Dissociative electron attachment to anthralin to model its biochemical reactions. *The Journal of Physical Chemistry Letters* **5**:2916–2921 DOI 10.1021/jz501523s.

Rodger R, Nordén B. 1997. *Circular dichroism and linear dichroism*. Oxford: Oxford University Press.

Sehgal VN, Verma P, Khurana A. 2014. Anthralin/dithranol in dermatology. *International Journal of Dermatology* **53**:e449–60.

Serr A, O'Boyle N. 2009. Convoluting UV-Vis spectra using oscillator strengths. *Available at http:// gausssum.sourceforge.net/ GaussSum_UVVis_Convolution.pdf* (accessed on 09 October 2019).

Smulevich G, Foggi P, Feis A, Marzocchi MP. 1987. Fluorescence excitation and emission spectra of 1, 8-dihydroxyanthraquinone-d_0 and -d_2 in *n*-octane at 10 K. *Journal of Chemical Physics* **87**:5664–5669 DOI 10.1063/1.453540.

Spanget-Larsen J, Hansen BKV, Hansen PE. 2011. OH stretching frequencies in systems with intramolecular hydrogen bonds: harmonic and anharmonic analyses. *Chemical Physics* **389**:107–115 DOI 10.1016/j.chemphys.2011.09.011.

Thulstrup EW, Michl J. 1989. *Elementary polarization spectroscopy*. New York: Wiley-VCH.

Van de Kerkhof PCM. 1991. Dithranol treatment for psoriasis: after 75 years, still going strong! *European Journal of Dermatology* **1**:79–88.

Yanai T, Tew D, Handy NA. 2004. New hybrid exchange–correlation functional using the Coulomb-attenuating method (CAM-B3LYP). *Chemical Physics Letters* **393**:51–57 DOI 10.1016/j.cplett.2004.06.011.

Zheng D, Zhang M, Zhao G. 2017. Combined TDDFT and AIM insights into photoinduced excited state intramolecular proton transfer (ESIPT) mechanism in hydroxyl and amino-anthraquinone solution. *Scientific Reports* **7**:13766 DOI 10.1038/s41598-017-14094-5.